scientific reports

OPEN

Evidence of a liquid–liquid phase transition in H$_2$O and D$_2$O from path-integral molecular dynamics simulations

Ali Eltareb[1,3]✉, Gustavo E. Lopez[2,4] & Nicolas Giovambattista[1,3,4]

We perform path-integral molecular dynamics (PIMD), ring-polymer MD (RPMD), and classical MD simulations of H$_2$O and D$_2$O using the q-TIP4P/F water model over a wide range of temperatures and pressures. The density $\rho(T)$, isothermal compressibility $\kappa_T(T)$, and self-diffusion coefficients $D(T)$ of H$_2$O and D$_2$O are in excellent agreement with available experimental data; the isobaric heat capacity $C_P(T)$ obtained from PIMD and MD simulations agree qualitatively well with the experiments. Some of these thermodynamic properties exhibit anomalous maxima upon isobaric cooling, consistent with recent experiments and with the possibility that H$_2$O and D$_2$O exhibit a liquid-liquid critical point (LLCP) at low temperatures and positive pressures. The data from PIMD/MD for H$_2$O and D$_2$O can be fitted remarkably well using the Two-State-Equation-of-State (TSEOS). Using the TSEOS, we estimate that the LLCP for q-TIP4P/F H$_2$O, from PIMD simulations, is located at $P_c = 167 \pm 9$ MPa, $T_c = 159 \pm 6$ K, and $\rho_c = 1.02 \pm 0.01$ g/cm^3. Isotope substitution effects are important; the LLCP location in q-TIP4P/F D$_2$O is estimated to be $P_c = 176 \pm 4$ MPa, $T_c = 177 \pm 2$ K, and $\rho_c = 1.13 \pm 0.01$ g/cm^3. Interestingly, for the water model studied, differences in the LLCP location from PIMD and MD simulations suggest that nuclear quantum effects (i.e., atoms delocalization) play an important role in the thermodynamics of water around the LLCP (from the MD simulations of q-TIP4P/F water, $P_c = 203 \pm 4$ MPa, $T_c = 175 \pm 2$ K, and $\rho_c = 1.03 \pm 0.01$ g/cm^3). Overall, our results strongly support the LLPT scenario to explain water anomalous behavior, independently of the fundamental differences between classical MD and PIMD techniques. The reported values of T_c for D$_2$O and, particularly, H$_2$O suggest that improved water models are needed for the study of supercooled water.

Water is an anomalous liquid with thermodynamic and dynamical properties that behave unexpectedly upon cooling and/or pressurization; see, e.g., Ref.[1]. For example, experiments performed in the 1970's by Angell et al.[2–4] show that water isobaric heat capacity $C_P(T)$ and isothermal compressiblity $\kappa_T(T)$ exhibit an apparent divergency at $T \approx 228$ K and $P = 0.1$ MPa. More recent experiments that extend Angell's studies to lower temperatures identify a maxima in $C_P(T)$ and $\kappa_T(T)$ at $T \approx 228$ K ($P = 0.1$ MPa)[5,6]. Although many theoretical approaches have been proposed to explain water anomalous behavior, the so-called liquid–liquid phase transition (LLPT) scenario[7,8] is currently the explanation best-supported by experiments[5,9–13], computer simulations[7,14–18], and theory[14,19–23]. In the LLPT scenario, water at low temperatures exists in two distinct liquid states, low-density and high-density liquid (LDL and HDL). In the P–T plane, LDL and HDL are separated by a first-order LLPT line that ends at a liquid–liquid critical point (LLCP) at higher temperatures. Importantly, the LLPT hypothesis explains naturally the maxima in $\kappa_T(T)$ and $C_P(T)$ observed recently upon cooling water at $P = 0.1$ MPa[5,10]. It also explains, naturally, the complex behavior of water in the glass state[8,9,24–34] which, arguably, is not clearly explained by other approaches, such as the singularity free scenario[35].

Available experimental data suggest that the LLCP in water is located at about $P_c = 50–100$ MPa and $T \approx 220$ K[1,12]. Unfortunately, due to water rapid crystallization at these conditions, the existence of the LLCP in water has not been confirmed in experiments. Strong evidence for the existence of a LLPT in water is available

[1]Department of Physics, Brooklyn College of the City University of New York, Brooklyn, New York 11210, USA. [2]Department of Chemistry, Lehman College of the City University of New York, Bronx, NY 10468, USA. [3]Ph.D. Program in Physics, The Graduate Center of the City University of New York, New York, NY 10016, USA. [4]Ph.D. Program in Chemistry, The Graduate Center of the City University of New York, New York, NY 10016, USA. ✉email: ali.eltareb@brooklyn.cuny.edu

from recent sub-microsecond experiments at $T \approx 205$ K[9]; additional evidence of the LLPT in water is available from experiments performed at $T \approx 130–140$ K, in the the so-called ultraviscous liquid state of water[36,37]. Many computer simulations validate the LLPT hypothesis. Specifically, a LLCP has been identified in classical computer simulations using popular models, such as ST2, TIP4P/2005, and TIP4P/ice[7,14,18,38–44]. A recent classical MD simulation using a water model developed from density functional theory combined with machine learning techniques also suggests that water exhibits a LLCP in the supercooled regime[21]. Not surprisingly, the location of the LLCP in computer simulations vary with the water model considered. For example, in the case of the ST2 water model, the LLCP temperature is overestimated ($T_c = 237$ K, $P_c = 167$ MPa, $\rho_c = 0.99$ g/cm³)[41]; while in the TIP4P/2005 and TIP4P/Ice water models it is underestimated ($T_c = 172$ K, $P_c = 186$ MPa, and $\rho_c = 1.03$ g/cm³ for TIP4P/2005; $T_c = 188$ K, $P_c = 175$ MPa, $\rho_c = 1.01$ g/cm³ for TIP4P/Ice)[18]. In all these cases, the LLCP pressure is overestimated by approximately 100 MPa[6]. The computer simulation studies that find a LLCP in water are based on classical models where the atoms delocalization due to nuclear quantum effects (NQE) are neglected. This can be troublesome because water is a light molecule and delocalization effects of its H atoms occur even at standard temperatures and pressures[45,46]. For example, the temperature of maximum density and the glass transition temperature (T_g) of H_2O and D_2O differ by 7–10 K, a clear sign of non-negligible NQE. Path-integral computer simulations of water-like models that have a LLCP clearly show that NQE can indeed shift the location of the LLCP as well as alter the shape and slope of the $C_P(T)$ and $\kappa_T(T)$ maxima lines[47,48]. Interestingly, while experiments in glassy water have estimated differences in the location of the LLCP in H_2O and D_2O ($\Delta T_c \approx 10$ K, $\Delta P_c \approx 50$ MPa)[49,50], the issue of isotope effects on the location of the LLCP has not been explored in computational and theoretical studies.

In this work we perform extensive path-integral, ring-polymer, and classical molecular dynamics (PIMD, RPMD, MD) simulations of light and heavy water using the q-TIP4P/F model and explore the corresponding phase diagram and thermodynamic/dynamical anomalous properties. One goal of this work is to determine the NQE (due to atoms delocalization) on the location of the LLCP, LLPT, and supercritical anomalous lines (such as maxima lines in ρ, C_P, and κ_T) in q-TIP4P/F water (H_2O). The second goal of this work is to study isotope substitution effects in water, i.e., whether PIMD simulations of H_2O and D_2O can reproduce the subtle differences in the phase diagram and anomalous properties of H_2O and D_2O observed in experiments. In a previous study, we performed PIMD simulations of q-TIP4P/F water at $P = 0.1$ MPa and showed that this model reproduces some signatures of the LLPT scenario, specifically, a maximum in $\kappa_T(T)$ was found in H_2O and D_2O at $T \approx$ 230–235 K ($P = 0.1$) MPa[46]. Here, we extend our previous study to a wide range of temperatures and pressures in order to explore the possible existence of a LLCP in H_2O and D_2O. By combining the PIMD/MD results and the two-state equation of state (TSEOS)[14,22,23], we are able to identify a LLCP in both H_2O and D_2O. The TSEOS is based on the assumption that liquid water is a mixture of two interconvertible (liquid) states. The TSEOS has been shown to fit remarkably well the computer simulations results obtained from classical MD simulations of ST2 and TIP4P/2005 water as well as a water model based on DFT and machine learning techniques[14,19–21,23]; it has also been applied to the case of real water[20,51]. While at low temperatures the TSEOS predicts that water separates into LDL and HDL, at high temperatures ($T > 270$ K), it predicts a rather homogeneous liquid (HDL) which is consistent with recent computer simulations[52,53].

Our paper is organized as follows. In "Simulation method", we present the computer simulation details. In "Results", we discuss the results from our PIMD/RPMD and classical MD simulations of H_2O using the q-TIP4P/F water model. The phase diagram of D_2O is briefly discussed and compared with the phase diagram of H_2O. A summary and discussions are included in "Summary and discussion".

Simulation method

Our results are based on PIMD/RPMD and classical MD simulations of a system composed of $N = 512$ water molecules in a cubic box with periodic boundary conditions. H_2O and D_2O molecules are represented using the non-rigid q-TIP4P/F model[54]. This model is based on the TIP4P/2005 model for water[55], commonly used in classical MD simulations. The q-TIP4P/F water model was optimized for path integral computer simulations and has been shown to be able to reproduce remarkably well the properties of liquid water at $P = 0.1$ MPa[46,54]. Here, we perform PIMD and MD simulations at constant N, P, and T over a wide range of temperatures and pressures, $180 \leq T \leq 375$ K and $-250 \leq P \leq 500$ MPa; see Supplementary Fig. S1 of the Supplementary Information (SI). The temperature of the system is maintained constant using a stochastic (local) path integral Langevin equation (PILE) thermostat[56] while the pressure of the system is controlled by using a Monte Carlo Barostat (additional computational details can be found in Ref.[46]). In the PIMD simulations, the time step dt is set to 0.25 fs and the number of beads per ring-polymer/atom was set to $n_b = 32$; in Ref.[46], it is shown that this value of n_b is large enough to obtain well-converged dynamical, thermodynamic, and structural properties of q-TIP4P/F water at $P = 0.1$ MPa and $T \geq 210$ K. In order to ensure that the conclusions in Ref.[46] applied to the pressures we considered in this work, we have also performed additional PIMD simulations using $n_b = 72$ beads per ring-polymer (see SI). Consistent with Ref.[46], we found that most of the thermodynamic and dynamical properties converged with $n_b = 32$, with the enthalpy being the only expected exception. Short-range (Lennard–Jones pair potential) interactions are calculated using a cutoff $r_c = 1.0$ nm and long range electrostatic interactions are computed using the Particle Mesh Ewald (PME) method with the same cutoff r_c. In the classical MD simulations, we employ a time step $dt = 0.50$ fs and set $n_b = 1$. All PIMD and classical MD simulations are performed using the OpenMM software package (version 7.4.0)[57]. The OpenMM software package is also used to perform the RPMD simulations which are used for the calculation of the diffusion coefficients of H_2O and D_2O. Details on the calculation of the diffusion coefficients can be found in Ref.[46]. We note that in the OpenMM software package, the RPMD application sets the mass of the ring-polymer beads to the physical mass of the corresponding atom. When used

	PIMD	Classical MD
P_c	167 (9)	203 (4)
T_c	159 (6)	175 (1)
ρ_c	1.02 (0.01)	1.03 (0.01)

Table 1. Estimated pressure P_c, temperature T_c, and density ρ_c of the LLCP of q-TIP4P/F H_2O. Values of P_c, T_c, and ρ_c are obtained by using the TSEOS in combination with data from classical MD and PIMD simulations at $180 \leq T \leq 325$ K. Numbers in parenthesis are standard deviations.

to calculate static equilibrium properties (energies, density, and RDF), the RPMD simulations reduce to PIMD simulations.

In all PIMD/RPMD and classical MD simulations, the system is equilibrated for a time interval t_{eq} followed by a production run of time length t_{prod}. The values of t_{eq} and t_{prod} depend on the state point simulated. Typical simulation times for PIMD/RPMD range from 2.5 ns to 100 ns. Simulation times for classical MD simulations range from 2.5 ns to 2–3 μs. To confirm that the system reaches equilibrium, we monitor the mean-square displacement (MSD) of the water molecules in the system as a function of time and confirm that the PIMD/RPMD and classical MD simulations satisfy the requirement that $t_{eq}, t_{prod} > \tau$, where τ is the time it takes for the MSD of water molecules to reach 1 nm^2.

Results

The results are presented as follows. In "Liquid–liquid phase transition", we show that the phase diagrams of H_2O from MD and PIMD simulations are consistent with the existence of a LLPT and LLCP at low temperatures. Since a LLCP generates anomalous loci of maxima in C_P and κ_T, the behavior of $C_P(T)$ and $\kappa_T(T)$ are discussed in "Thermodynamic response functions: κ_T and C_p". The self-diffusion coefficient of H_2O and D_2O are the topic of "Diffusion coefficient" where we identify the anomalous locus of diffusivity maxima. A complete phase diagram for H_2O is presented in "Phase diagram" where we also discuss similar results obtained for D_2O.

Liquid–liquid phase transition. Figure 1a shows the density of H_2O from both classical MD (open circles) and PIMD simulations (solid circles) along the isobars $P = -100, 0.1, 100, \ldots, 500$ MPa and at temperatures in the range $T = 180–375$ K. The densities from MD and PIMD simulations overlap practically throughout the entire temperature and pressure range considered with some deviations being noticeable only at $P = 100–200$ MPa and $T < 240$ K. As we will show below, these T–P conditions are in the proximity of the LLCP. We note that the densities of q-TIP4P/F H_2O are in remarkable good agreement with the corresponding experimental values. To show this, we include in Fig. 1b the densities from experiments and PIMD simulations of q-TIP4P/F H_2O. Deviations between experiments and PIMD simulations are small, $\Delta\rho < 0.02–0.03$ g/cm^3, and are present only at $P > 200$ MPa and $T < 250$ K (similar values of $\Delta\rho$ hold for the case of MD simulations). It follows that both MD and PIMD simulations of q-TIP4P/F water predict the correct location (T and P) for the density maximum of water. In these and other cases, the computer simulation results can be fitted remarkably well using the TSEOS[14,20–23,58]. In Fig. 1c,d, we compare the $\rho(T)$ isobars obtained from the MD and PIMD simulations of q-TIP4P/F water with the corresponding fit using the TSEOS (a brief explanation of the methodology used to obtain the TSEOS can be found in Refs.[14,21]). The TSEOS is fitted using only the PIMD and MD data for $180 \leq T \leq 325$ K and $-50 \leq P \leq 350$ MPa. As shown in Fig. 1c,d, the TSEOS isobars are in excellent agreement with the simulation results over a majority of the state points simulated. Interestingly, the TSEOS also predicts a minimum in the $\rho(T)$ isobars of q-TIP4P/F water. While at the studied temperatures we do not observe density minima in the classical MD and PIMD simulations, density minima were reported at different pressures in TIP4P/2005 and ST2 water[15,42]. The optimized parameters for the TSEOS are given in Table S1 of the SI.

The TSEOS also provides a good estimation of the LLCP location. For example, in the case of TIP4P/2005 water, the TSEOS predicts that $T_c = 182$ K, $P_c = 170$ MPa, and $\rho_c = 1.02$ g/cm^3[14], which is in good agreement with recent MD simulations that were able to access the LLCP, $T_c = 172$ K, $P_c = 186$ MPa, and $\rho_c = 1.03$ g/cm^3[18]; similar results were found in an MD simulation study combined with the potential energy landscape theoretical approach[43]. Using the TSEOS, one can estimate the LLCP location (ρ_c, T_c, P_c). The values of (ρ_c, T_c, P_c) for the case of q-TIP4P/F H_2O, based on classical MD and PIMD simulations, are given in Table 1 and are indicated in Fig. 1c,d by a red star. It follows that including NQE can shift the location of the LLCP. Specifically, relative to the classical case (MD simulations), adding NQE (PIMD simulations) lowers T_c and P_c by 16 ± 6 K, 36 ± 10 MPa, respectively; ρ_c is not affected by the inclusion of NQE. Interestingly, recent studies based on water-like mono-atomic model liquids that exhibit a LLCP, show that including NQE has the effects of lowering T_c and increasing P_c, while leaving ρ_c unaffected[47,48].

We also compare the volumes predicted by the TSEOS with the corresponding values obtained from our MD and PIMD simulations. Fig. 2a,b show $P(V)$ along isotherms based on the classical MD and PIMD simulations, respectively. In both cases, MD and PIMD simulations, the values of $P(V)$ obtained from the TSEOS are in excellent agreement with our simulations. This strongly indicates that the TSEOS is reliable in predicting the properties of q-TIP4P/F water from both MD and PIMD simulations. We note that the $P(V)$ isotherms shown in Fig. 2a,b seem to develop an inflection point as the temperature decreases, consistent with the existence of a LLCP at $T < 200$ K. Similarly, as shown in Fig. 2c, the potential energy $PE(V)$ along isotherms is an increasing function of V at high temperatures but it develops a concave region (i.e., $\left(\partial^2 PE/\partial V^2\right)_{N,T} < 0$) at low
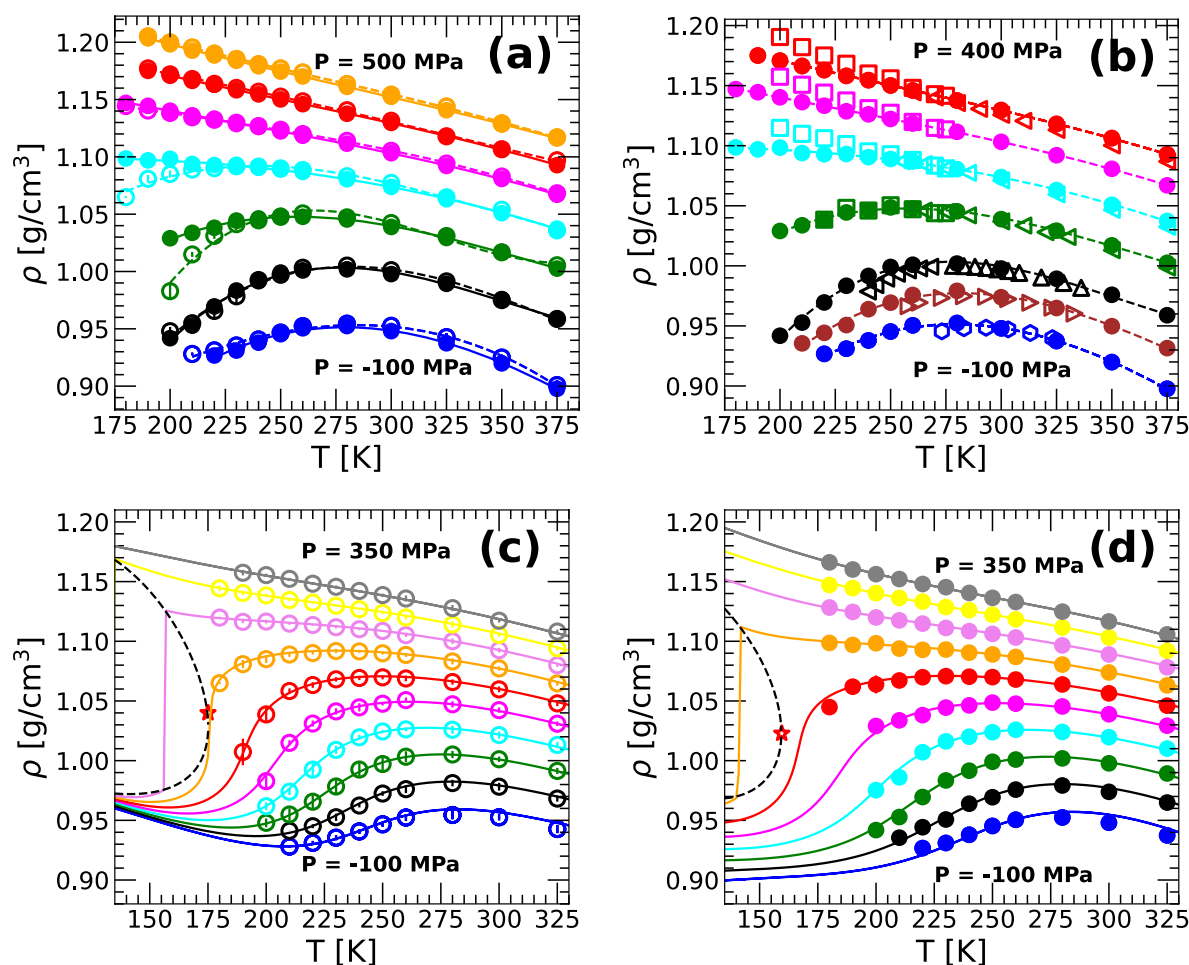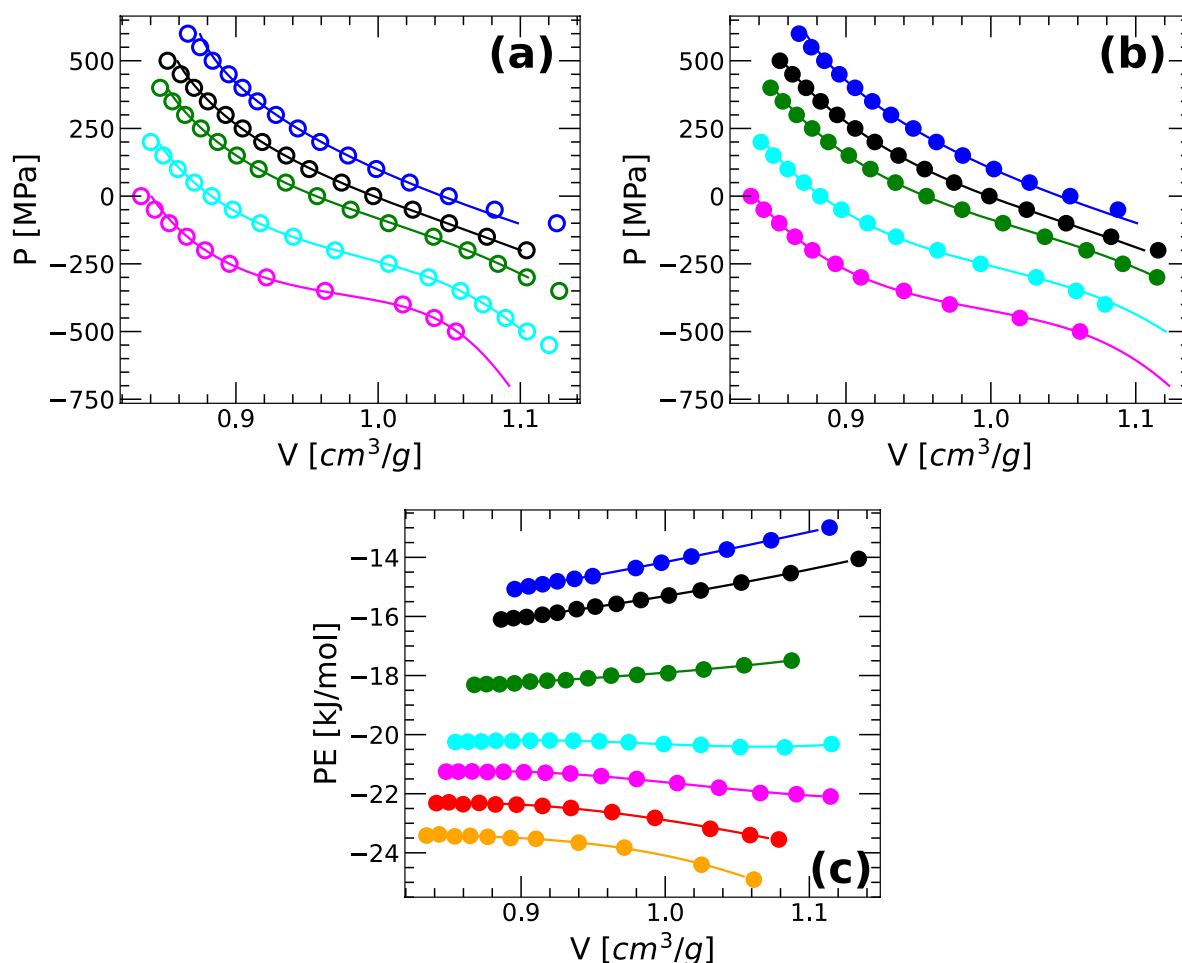
Figure 1. Density of q-TIP4P/F water as function of temperature along selected isobars. (**a**) Comparison of $\rho(T)$ from classical MD (open circles) and PIMD simulations (solid circles). Pressures are (bottom to top) $P = -100, 0.1, 100, 200, 300, 400, 500$ MPa. (**b**) Density of q-TIP4P/F water from PIMD simulations (solid circles) and experiments (open symbols; squares, left-triangles, up-triangles, right-triangles, and diamonds are, respectively, from Refs.[12,16,59–61]). Pressures are (bottom to top) $P = -100, -50, 0.1, 100, 200, 300, 400$ MPa. Deviations between experiments and simulations are noticeable only at high pressures, $P > 200$ MPa, and low temperatures, $T < 240$ K. (**c**) Fit of the q-TIP4P/F water densities shown in (**a**) using the TSEOS (solid lines). (**d**) Fit of the q-TIP4P/F water densities shown in (**b**) using the TSEOS (solid lines). Pressures in (**c**) and (**d**) are (bottom to top) $P = -100, -50, 0.1, 50, 100, 150, 200, 250, 300, 350$ MPa. The liquid–liquid binodal line and LLCP predicted from the TSEOS are denoted by the black dashed line and red star.

temperatures. The Helmholz free energy of the system is $F(N, V, T) = E - TS$ and hence, a concavity in PE can lead to a concavity in $F(V)$ (at constant N and T) at very low temperatures. A concavity in $F(V)$ implies that the system exhibits a first-order (liquid–liquid) phase transitions[62], again, consistent with the presence of LLCP/LLPT at low temperatures.

Thermodynamic response functions: κ_T and C_p. We obtain the isothermal compressibility of q-TIP4P/F water by calculating the density fluctuations of the system[63],

$$\kappa_T(T) = \frac{\langle V^2 \rangle - \langle V \rangle^2}{k_B T \langle V \rangle}, \tag{1}$$

where $\langle \ldots \rangle$ indicates average over time and k_B is the Boltzmann's constant. Fig. 3a,b show the $\kappa_T(T)$ for H_2O obtained from PIMD simulations (solid circles) together with available experimental data (open symbols) at low and high pressures, respectively. At $P \geq 200$ MPa (Fig. 3b), the experimental and PIMD simulation values of $\kappa_T(T)$ practically overlap; a similar agreement is found at $P = 100$ MPa (Fig. 3a). However, at $P = 0.1$ MPa, where more experimental data is available, the experimental $\kappa_T(T)$ increases more rapidly upon cooling than found in PIMD simulations. Hence, relative to real water, the density fluctuation in q-TIP4P/F water are underestimated at $P = 0.1$ MPa and in the supercooled regime. We note that the values of $\kappa_T(T)$ obtained from classical MD

Figure 2. Pressure of q-TIP4P/F water as a function of volume along selected isotherms. Circles are results from (**a**) classical MD and (**b**) PIMD simulation. The solid lines are the results from the TSEOS. Isotherms correspond to (top to bottom) $T = 300, 260, 240, 220, 200$ K and are shifted by $\delta P = 100, 0, -100, -300, -500$ MPa, respectively. An inflection point in $P(V)$ seems to develop at $T < 200$ K consistent with the existence of a LLPT in q-TIP4P/F water at lower temperatures. (**c**) Potential energy for selected isotherms at (bottom to top) $T = 200, 220, 240, 260, 300, 350, 375$ K. Solid symbols are from PIMD simulations; lines are guides to the eye.

and PIMD simulations overlap (within error bars) at $T \geq 190$ K and hence, they were omitted in Fig. 3a,b; the $\kappa_T(T)$ obtained from MD simulations is shown in Fig. S2 of the SI.

An important result from Fig. 3a is the presence of maxima in $\kappa_T(T)$ at $P = 0.1$ and 100 MPa. This is an anomalous property that was originally predicted by the LLPT hypothesis scenario and later confirmed by experiments[5,17]. The experimental data from Ref.[5] is included in Fig. 3a; the experimental κ_T-maximum occurs at $T = 228$ K ($P = 0.1$ MPa; open right triangles) and it is very sharp. While the κ_T-maximum in PIMD simulations occurs at a similar temperature ($T = 230$ K), this maximum is much smaller and wider relative to the experiments. Within the LLCP hypothesis scenario, the κ_T-maximum is expected to increase as one approaches the LLCP and it should diverge at the LLCP. This is fully consistent with the PIMD simulations results shown in Fig. 3a. Specifically, as the pressure increases from $P = 0.1$ MPa to $P = 100$ MPa, the κ_T-maximum shifts to lower temperatures and increases in height. The same behavior of κ_T is found in classical MD simulations of water models that exhibit a LLCP[14,15,21,64].

We also calculate $\kappa_T(T)$ using the TSEOS. The TSEOS provides an expression for the Gibbs free energy of the system from which the isothermal compressibility can easily be obtained,

$$\kappa_T(T) = -\frac{\left(\partial^2 G/\partial P^2\right)_T}{\left(\partial G/\partial P\right)_T}. \tag{2}$$

A comparison of the values of $\kappa_T(T)$ obtained from the TSEOS and our MD/PIMD simulations are presented in Fig. 3c,d. The predictions from the TSEOS agree rather well with the MD simulation results [inset of Fig. 3d]. In the case of PIMD simulations [inset of Fig. 3c], the TSEOS provides compressibility values that are in good
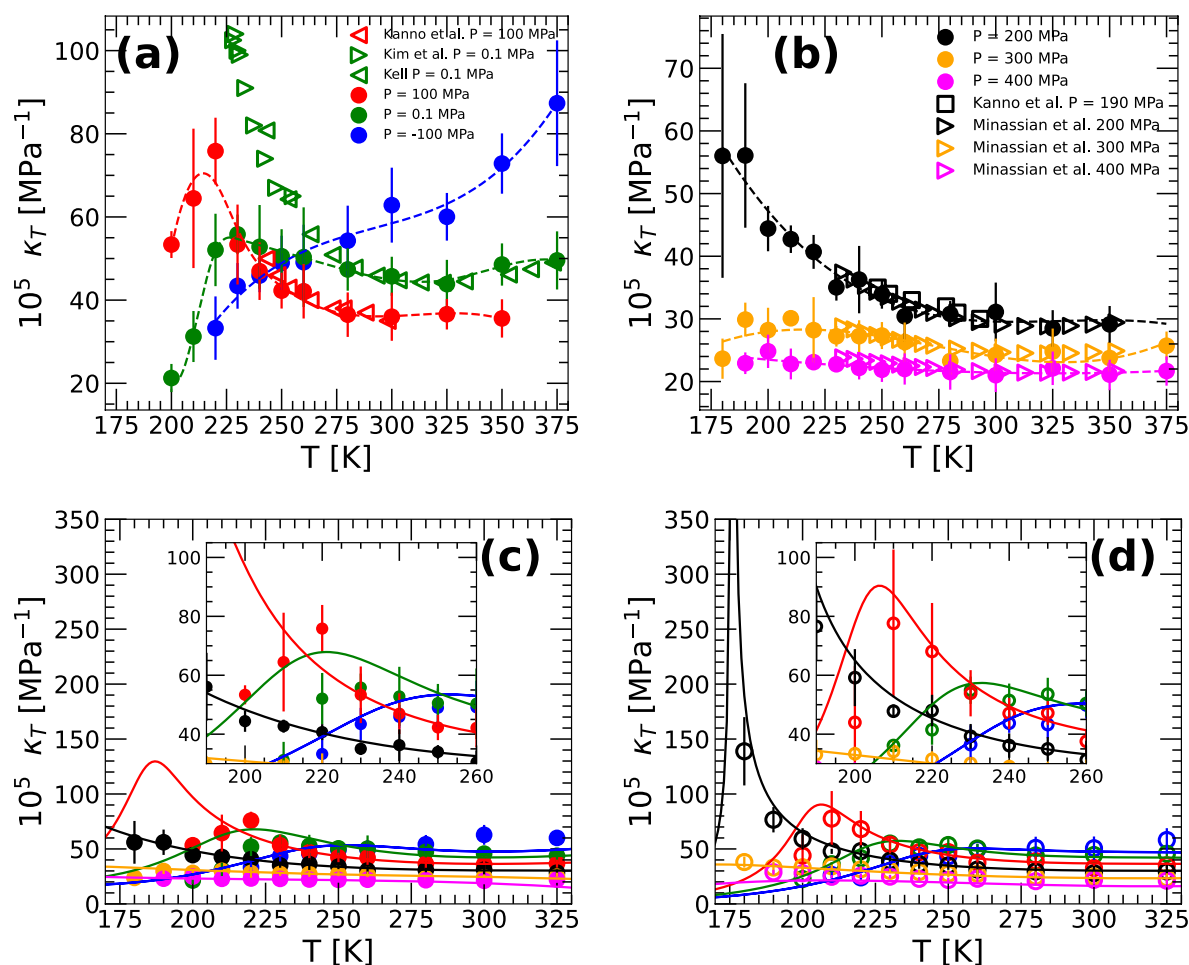
Figure 3. (**a**) Isothermal compressibility of q-TIP4P/F water from PIMD simulations at pressures $P = -100,\ 0.1, 100$ MPa (solid circles; dashed lines are guides to the eye). Experimental data for $\kappa_T(T)$ are indicated by open symbols (red left-triangles, green left- and right-triangles are from Refs.[5,65,66], respectively). (**b**) Same as (**a**) for pressures $P = 200,\ 300,\ 400$ MPa; experimental values of $\kappa_T(T)$ are from Refs.[65,67]. (**c**) Comparison between the values of $\kappa_T(T)$ obtained from the PIMD simulations [solid circles; from (**a**) and (**b**)] and the TSEOS (solid lines). (**d**) Comparison between the values of $\kappa_T(T)$ obtained from the MD simulations (empty circles) and the TSEOS (solid lines). Insets are magnifications of the main panels. The predictions of the TSEOS are in very good agreement with the MD simulation results and semiquantitative agreement in the case of PIMD simulations.

agreement with the simulation results at high temperatures. However, at lower temperatures, the TSEOS predicts slightly larger maxima in κ_T that are shifted to lower temperatures relative to the simulations. This suggests that, the location of the LLCP in q-TIP4P/F water from PIMD may be located at slightly lower T_c and/or higher P_c relative to the corresponding *estimated* values resulting from the TSEOS.

Next, we discuss the isobaric heat capacity,

$$C_P(T) = \left(\frac{\partial H(T)}{\partial T}\right)_{N,P}. \tag{3}$$

In our previous work (at $P = 0.1$ MPa)[46], the enthalpy was calculated directly from MD and PIMD simulations at selected temperatures and then, the values of $H(T)$ were fitted using a fourth-order polynomial. The resulting analytic expression for $H(T)$ was then used in Eq. (3) to calculate $C_P(T)$. The use of a fourth-order polynomial in the fitting procedure is rather arbitrary. It captures the qualitative increase of $C_P(T)$ upon cooling at low pressures but it may play a relevant role in identifying a C_P-maximum, which is known to occur in experiments[10]. Accordingly, in this work, we take advantage of the TSEOS and use it to calculate $H(T)$ at selected pressures; after all, the TSEOS reproduces very well the behavior (and maxima) of $\rho(T)$ (see Fig. 1) and $\kappa_T(T)$ (see Fig. 3). Specifically, for a given pressure, we use the polynomial expression of $G(T)$ given by the TSEOS and obtain an analytical expression for $H(T)$ using the Gibbs–Helmholtz equation,
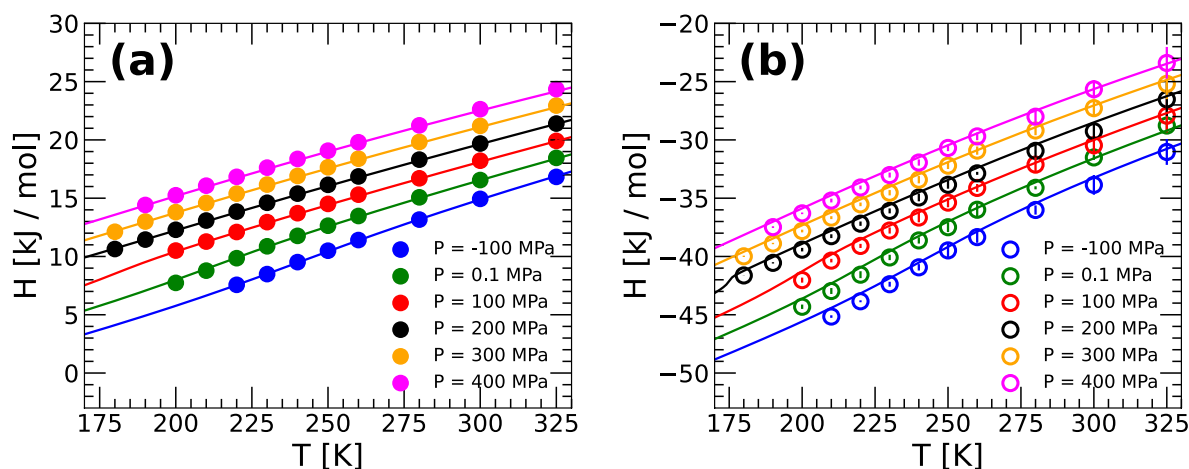
Figure 4. Enthalpy $H(T)$ of q-TIP4P/F water as a function of temperature for selected pressures. Results are from (**a**) PIMD simulations (solid circles) and (**b**) classical MD simulations (empty circles). Lines are the corresponding $H(T)$ obtained from the TSEOS. In both cases, the TSEOS predictions are in excellent agreement with the MD/PIMD simulation results.
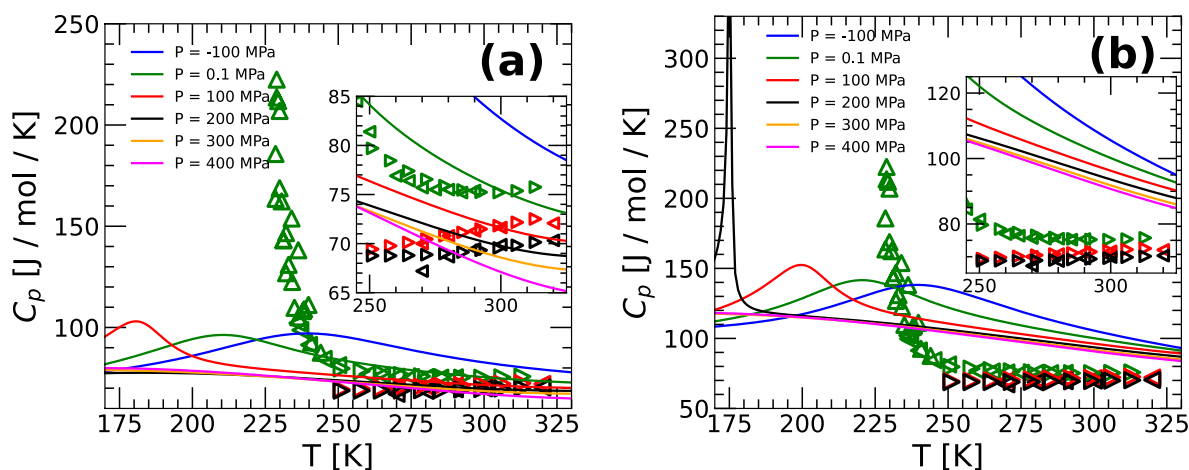

Figure 5. (**a**) Heat capacity $C_P(T)$ of q-TIP4P/F water for P = -100, 0.1, 100, 200, 300, and 400 MPa. $C_P(T)$ was calculated by using Eq. (3) and the $H(T)$ expression obtained from the TSEOS and PIMD simulations (solid lines). Experimental data are indicated by empty triangles (left-triangles from Refs.[4,69]; right-triangles from Refs.[59]). (**b**) Same as (**a**) for the case of classical MD simulations. The experimental data from Pathak et al.[10] (green up-triangles) show a maximum at $T \approx 228$ K.

$$H(T) = -T^2 \left(\frac{\partial (G/T)}{\partial T} \right)_P. \tag{4}$$

The obtained $H(T)$ is then used in Eq. (3) to calculate $C_P(T)$. Figure 4a,b show the $H(T)$ of q-TIP4P/F water obtained from (i) the TSEOS (solid lines) and (ii) classical MD and PIMD simulations (empty/solid circles). The TSEOS predictions are in excellent agreement with our simulations throughout the entire temperature and pressure range considered in this work.

Figure 5a,b show, respectively, the $C_P(T)$ of q-TIP4P/F water from PIMD and classical MD simulations at selected pressures, above and below the estimated LLCP pressure; open symbols are experimental values. The $C_P(T)$ from classical MD and PIMD simulations are qualitatively similar. Specifically, at the temperature studied, $C_P(T)$ exhibits a maximum at approximately $P \leq 200$ MPa. This C_P-maximum increases and shifts to lower temperatures as the pressure increases towards the LLCP pressure. At $P > 200$ MPa $> P_c$, $C_P(T)$ is a monotonic decreasing function of T. Note that classical MD simulations predict much larger values of $C_P(T)$ than found in PIMD simulations (which is known to occur when NQE are omitted[68]).

Differences between the experimental data and MD/PIMD simulations are noticeable. For example, as shown in Fig. 5a, at $P \geq 100$ MPa, PIMD simulations predict that $C_P(T)$ decreases upon heating while experiments show the opposite behavior. In particular, at $P = 0.1$ MPa, the $C_P(T)$ of q-TIP4P/F water is in semiquantitative
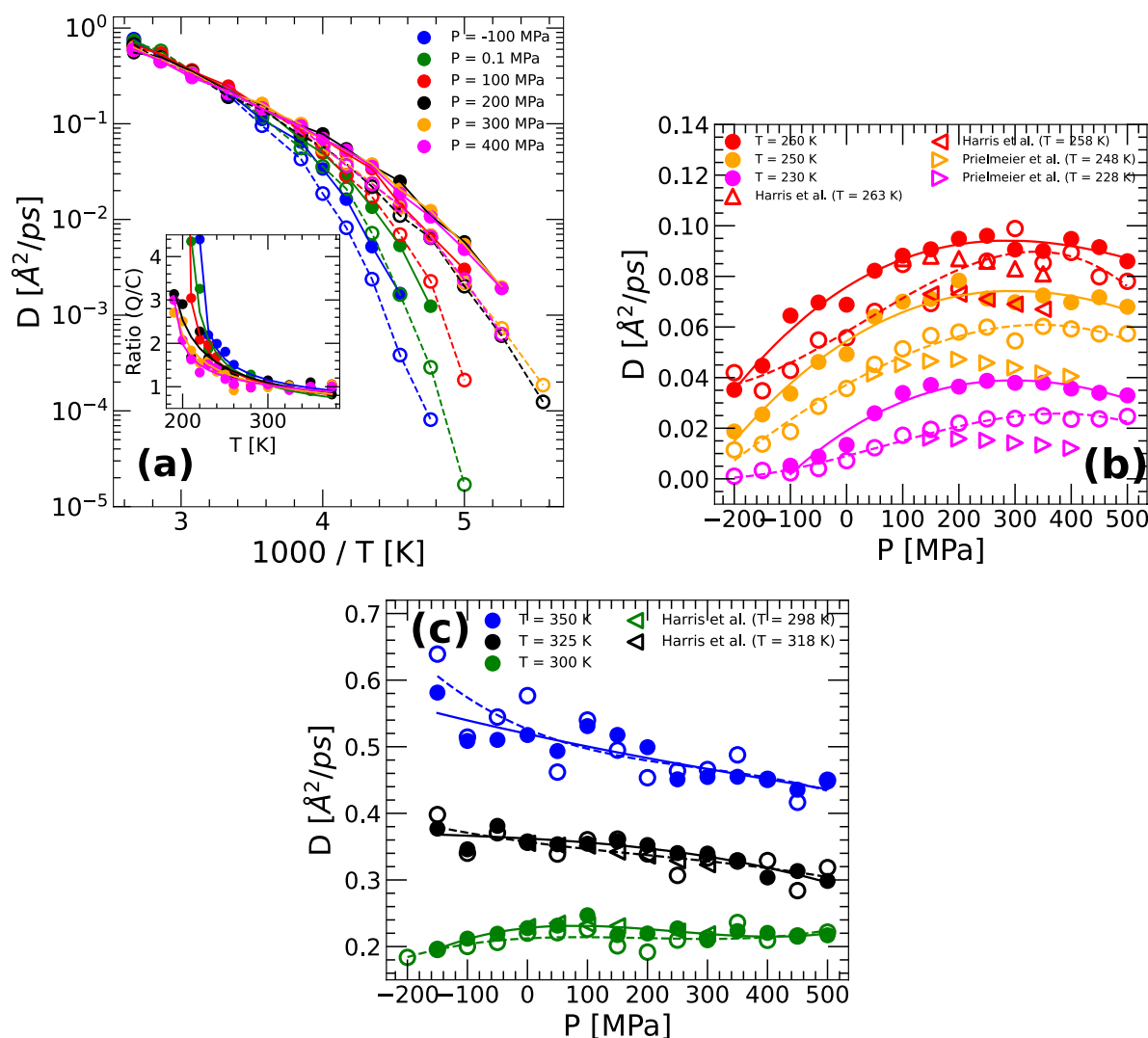
Figure 6. (**a**) Diffusion coefficient of q-TIP4P/F water as function of temperature at selected pressures. Results from RPMD simulations are indicated by solid circles; empty circles are results from classical MD simulations. Inset: ratio of the diffusion coefficients obtained from RPMD and MD simulations shown in the main panel. The inclusion of NQE increases water dynamics upon supercooling. (**b,c**) Diffusion coefficients of q-TIP4P/F water as function of pressure obtained from RPMD (solid circles) and classical MD simulations (empty circles); empty triangles correspond to experimental data (left-triangles and right-triangles from Refs.[70,71], respectively). An anomalous diffusivity maximum exist in q-TIP4P/F water at approximately $T < 300$ K.

agreement with experiments down to $T \approx 240$ K. The maximum in $C_P(T)$, at $P = 0.1$ MPa, occurs at 228 K and 216 K in experiments and q-TIP4P/F water, respectively. However, the maxima of $C_P(T)$ in q-TIP4P/F water is much smaller and wider than found in the experiments of Pathak et al.[10]. This is consistent with the estimated location of the LLCP in experiments and in our simulations. The LLCP in real water is estimated to be located at $P_C \approx 50$–100 MPa and $T_C \approx 220$ K, while in q-TIP4P/F water we find $T_c = 159$ K and $P_c = 167$ MPa. Accordingly, at $P = 0.1$ MPa, experiments are much closer to the corresponding LLCP than in the case of q-TIP4P/F water[6]. Our results for $C_P(T)$ also imply that PIMD and MD simulations of q-TIP4P/F water cannot reproduce the entropy fluctuations observed in real water at low temperatures and pressures.

Diffusion coefficient. We also calculate the self-diffusion coefficient of q-TIP4P/F water $D(T)$ as function of temperature at selected pressures. To obtain $D(T)$, we employ the same methodology used in Ref.[46]. Briefly, using the RPMD simulation technique, we first calculate the mean-square displacement (MSD) of the oxygen atoms/ring-polymer centroids. $D(T)$ is then evaluated from the slope of the MSD at long times, in the so-called diffusive regime. Figure 6a shows the $D(T)$ of q-TIP4P/F water obtained from RPMD (solid circles) and classical MD (open circles) simulations. At high temperatures, $D(T)$ is Arrhenius at all pressures studied, i.e.,
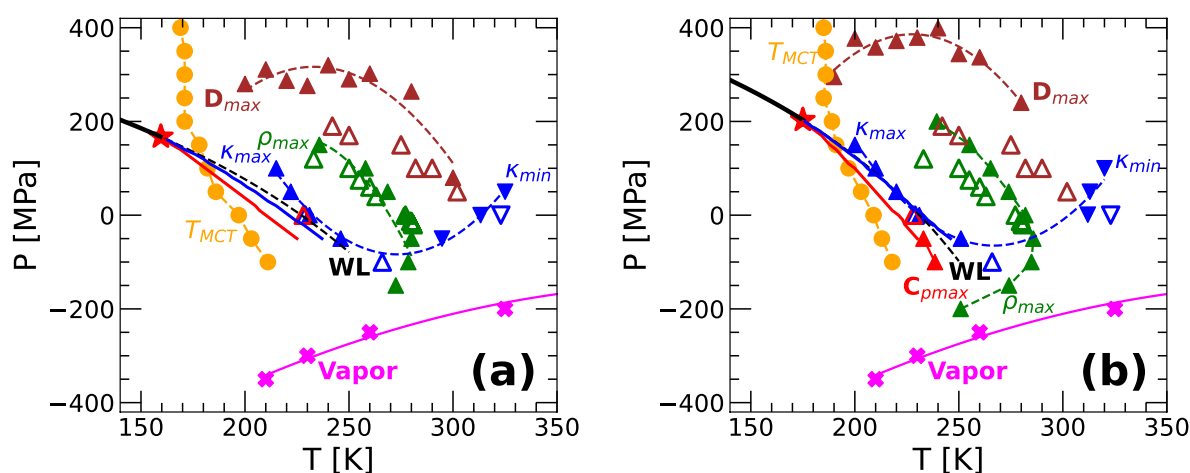
Figure 7. Phase diagram of q-TIP4P/F H_2O obtained from (**a**) PIMD/RPMD and (**b**) classical MD simulations. The black solid and dashed lines are, respectively, the LLPT and Widom lines obtained from the TSEOS; the filled red star is the LLCP from the TSEOS. The red and blue solid lines are the C_P-maxima and κ_T-maxima line from the TSEOS. The magenta crosses represent the vaporization line where the liquid spontaneously cavitates during the computer simulations. The green up-triangles are the density maxima. Blue up and down triangles represent, respectively, the maxima and minima in the isothermal compressibilities; red triangles indicate the maxima in C_P. Brown up-triangles are the maxima in the diffusion coefficient; orange circles represent the MCT temperature (see Eq. 5). Experimental data are shown by empty triangles[5,19,71,78–80]; filled symbols are results from MD/PIMD simulations. The estimated location of the LLCP based on experiments is (T_c = 220 K, P_c = 50–100 MPa)[12].

$$D(T) = D_1 exp\left(-\frac{E_A}{k_B T}\right), \qquad (5)$$

where D_1, E_A are constants; k_B is the Boltzmann constant. At low temperatures, the behavior of $D(T)$ depends on the pressure. Specifically, at high pressures, $P \geq 200$ MPa, in the HDL domain, $D(T)$ is non-Arrhenius and its behavior is well described by Mode Coupling Theory (MCT), i.e.,

$$D(T) = D_0(T - T_{MCT})^\gamma, \qquad (6)$$

where D_0, γ, and the MCT temperature T_{MCT} are constants. At low pressures (< 200 MPa), $D(T)$ also obeys MCT but only down to approximately $T = 200$–220 K. Upon further cooling, $D(T)$ seems to exhibit a crossover from non-Arrhenius ($T > 200$–220 K) to Arrhenius ($T < 200$ K) behavior. An Arrhenius regime at low temperatures can be identified in Fig. 6a for the case $P = -100$ MPa; the cases of $P = 100, 0.1$ MPa are less evident due to the limited available data at $T < 200$ K.

The values of D from the MD/PIMD simulations are compared with the corresponding experimental values in Fig. 6b,c along different isotherms. At high temperatures, approximately $T > 300$ K (Fig. 6c), the values of $D(P)$ from classical MD and PIMD simulations practically overlap with the available experimental data at all pressures studied. Instead, at $T < 300$ K (Fig. 6b), our simulation results predict values of $D(P)$ that deviate by up to a factor of 4 from the corresponding experimental data, depending on pressure. Interestingly, overall, classical MD simulations are in slightly better agreement with experiments compared to the RPMD simulation results. Not surprising, as shown in the inset of Fig. 6a, the inclusion of NQE increases water diffusivities, particularly upon cooling within the supercooled regime.

One of the main points of Fig. 6b is the presence of an anomalous maximum in the diffusion coefficient of q-TIP4P/F water. Such a D-maximum is consistent with experiments and implies that there is a range of temperatures at which D increases (anomalously) with increasing P.

Phase diagram. Figure 7a,b show, respectively, the phase diagram of q-TIP4P/F water obtained from PIMD and classical MD simulations. These phase diagrams include the LLCP, coexistence line, C_P-maxima, κ_T-maxima, and Widom line calculated from the TSEOS. Also included are the lines of ρ-maxima, D-maxima, C_P-maxima, κ_T-maxima, and κ_T-minima obtained from our MD/PIMD simulations. We also show the maxima/minima of these properties reported in experiments, where available. The liquid-vapor boundary lines shown in Fig. 7a,b correspond to the conditions at which spontaneous cavitation occurs during our computer simulation.

The phase diagrams of q-TIP4P/F water resulting from the classical MD and PIMD simulations are qualitatively similar. As found previously in ST2[42] and TIP4P/2005 water[15], the C_P and κ_T-maxima lines obtained from the TSEOS originate at the LLCP and deviate from each other at higher temperatures. The κ_T-maxima line (blue up-triangles) connects smoothly with the κ_T-minima line (blue down-triangles). In addition, as shown in Ref.[35], the point in Figs. 7 and 8 where the ρ-maxima line has infinite slope is located on the κ_T-extrema line, at which $(\partial \kappa_T / \partial T)_P = 0$. The ρ-maxima line has a nose shape. In particular, our simulations suggest that, at low pressures, the ρ-maxima line is re-entrant and deviates from the liquid-vapor boundary line [see, in particular,
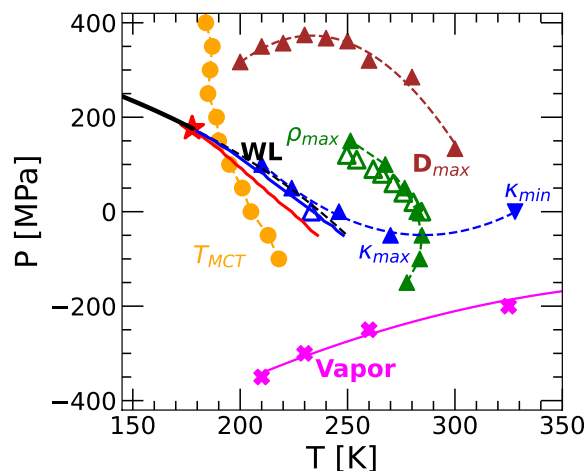
Figure 8. Same as Fig. 7 for the case of D_2O. Results are from PIMD/RPMD simulations using the q-TIP4P/F water model. The empty green-up triangles are experimental maxima densities from Ref.[81]. The empty blue-up triangle is the isothermal compressibility maxima from Ref.[5]. The estimated location of the LLCP based on experiments is ($T_c = 230$ K, $P_c = 50$ MPa)[50].

Fig. 7b]. This implies that the 're-entrant spinodal' hypothesis scenario proposed to explain water anomalous behavior is not supported by MD/PIMD simulations of q-TIP4P/F water. Hence, our results are consistent with Refs.[7,72], where computer simulations performed using the ST2 and TIP4P water model found that the spinodal line is also not re-entrant. We note that Fig. 7a,b also include available experimental data. When compared with experiments, both classical MD and PIMD reproduce correctly the location of the κ_T-maxima and minima lines; the PIMD simulation results reproduce slightly better the location of the ρ-maxima line.

Regarding the D-maxima line, both MD and RPMD simulations overestimate the corresponding pressures relative to the experiments, with the RPMD simulations performing slightly better. We also include in Fig. 7a,b the MCT temperatures extracted from Fig. 6a. The experimental MCT temperature at $P = 0.1$ MPa is $T_{MCT} = 221$ K[73] and hence, this temperature is underestimated in both MD and RPMD simulations.

Overall, the results from classical MD simulations in Fig. 7b are consistent with the TSEOS. Accordingly, one may conclude that the reported location of the LLCP based on the TSEOS is robust in the case of classical MD simulations. For example, the κ_T-maxima from MD simulations and from the TSEOS (blue triangles and blue solid lines) overlap; similarly, the corresponding C_P-maxima lines (red triangles and red solid lines) also overlap. In addition, we find that the $T_{MCT}(P)$ line shows a sudden change in slope at the intersection with the Widom line. This is consistent with the view that the Widom line separates the LDL-like liquid at low pressures from the HDL-like liquid at high pressures. The sharp crossover in $T_{MCT}(P)$ is reminiscent of the glass transition temperature of water as a function of pressure which shows a sudden change as the system evolves from LDL (low pressure) to HDL (high pressure)[31,74,75].

In the case of PIMD simulations (Fig. 7a), the κ_T-maxima line obtained from the TSEOS (blue solid line) is located at slightly lower pressure relative to the PIMD simulation results (blue up-triangles). Similarly, the Widom line predicted by the TSEOS is located at a pressure slightly lower than the pressure at which the slope of $T_{MCT}(P)$ suddenly changes. Hence, in the case of PIMD simulations for water, the reported location of the LLCP may shift slightly if additional data points at $T < 180$ K are considered in the TSEOS calculation. Additional PIMD simulations are also needed to improve the determination of the κ_T-maxima line at low temperatures.

The similarities in the phase diagrams of Fig. 7a,b imply that, at least for the q-TIP4P/water model, the LLPT hypothesis scenario remains a solid, viable explanation of water anomalous behavior even if NQE (i.e., atoms delocalization) are included. This is important since (i) the LLCP scenario has been tested only in classical MD simulations and, mostly, rigid water models, and (ii) the location of the LLCP is extremely sensitive to small variations in the water model considered (e.g., small changes in the partial charges of the H and O atoms can easily shift the location of the LLCP to (P, T) conditions that are physically inaccessible to the liquid state; see, e.g., Refs.[76,77]). Overall, including NQE shifts the location of the LLCP, LLPT line, and maxima/minima lines towards lower temperatures (see also Ref.[47,48]).

So far, our discussion has been centered on H_2O. The same analysis presented here for H_2O was done for the case of D_2O by performing PIMD simulations using the q-TIP4P/F model. The analogous to Figs. 1, 2, 3, 4, 5 and 6 are included in Figs. S4–S8 of the SI. Here, we only discuss the phase diagram of q-TIP4P/F D_2O; see Fig. 8. The phase diagram of D_2O is qualitatively similar to the phase diagram of H_2O. The LLCP in q-TIP4P/F D_2O is located at ($\rho_c = 1.13$ g/cm^3, $P_c = 176$ MPa, $T_c = 177$ K). Relative to q-TIP4P/F H_2O, the LLCP in D_2O is shifted by ($\Delta\rho_c \approx 0.11$ g/cm^3, $\Delta P_c \approx 9$ MPa, $\Delta T_c \approx 18$ K). Accordingly, our results indicate that isotope substitution in water can play an important role in the phase behavior of low-temperature and supercooled water. These values of ΔT_c and ΔP_c are consistent with the locations of the LLCP in H_2O and D_2O *estimated* by Mishima and Stanley from decompression-induced experiments of ice IV[49,50] where ($\Delta P_c \approx 50$ MPa, $\Delta T_c \approx 10$ K).

Summary and discussion

We performed classical MD, PIMD, and RPMD simulations of H_2O using the q-TIP4P/F model over a wide range of temperatures and pressures. At supercritical temperatures, most properties studied are practically insensitive to whether one employs classical MD and PIMD simulations ($-100 \leq P \leq 500$ MPa). Specifically, the $\rho(T)$ and $\kappa_T(T)$ obtained from classical MD or PIMD simulations overlap (within error bars) down to $T \approx 225$ K and $T \approx 200$ K, respectively (Fig. 1 and Fig. S2 of the SI). In the case of $C_P(T)$, the quantitative values vary for classical MD and PIMD results, but this is expected to occur due to NQE[68]. Nonetheless, the qualitative behavior of $C_P(T)$ is independent on whether NQE are included or excluded. Similarly, the behavior of $D(T)$ is not affected whether one employs classical MD or RPMD simulations down to $T \approx 260$ K (Fig. 6a). Relative to the classical MD simulations, including NQE (RPMD simulations) increases the values of $D(T)$ at $T < 260$ K (inset of Fig. 6a). In both cases, the $D(T)$ from computer simulations are in good agreement with experiments where data is available (Fig. 6b,c).

Deviations between MD and PIMD simulations become noticeable at approximately $P = 100–200$ MPa and $T < 225$ K. Our results strongly indicate that at these thermodynamic conditions, q-TIP4P/F water exhibits a LLCP. Using a two-state equation of state, we estimate that the LLCP is located at ($\rho_c = 1.03$ g/cm^3, $P_c = 203$ MPa, $T_c = 175$ K) when NQE are not included (classical MD); including NQE (PIMD simulations) shifts the location of the LLCP to ($\rho_c = 1.02$ g/cm^3, $P_c = 167$ MPa, $T_c = 159$ K); see Fig. 1c,d. Consistent with the existence of a LLCP, our study shows the presence of loci of maxima in C_P and κ_T in the P–T phase diagram of q-TIP4P/F water. These anomalous maxima lines, together with the loci of maxima in D and ρ are included in Fig. 7. We stress that the location of the LLCPs reported in this work are estimations provided by the TSEOS. Our estimation of the LLCP for H_2O is based on PIMD simulations using $n_b = 32$ beads per ring-polymer. While PIMD simulations with $n_b > 32$ are computationally expensive, additional PIMD simulations employing $n_b > 32$ beads per ring-polymer are desirable at low temperatures in order to obtain a more precise estimation of the LLCP location in H_2O (q-TIP4P/F water). While our results conclusively show that the LLCP in H_2O shifts to lower T when NQE are included, obtaining the exact values of (ρ_c, T_c, P_c) may require additional data at $T < 180$ K (particularly for the case of PIMD simulations of H_2O where T_c is low).

Overall, our results for H_2O (e.g., Fig. 7) are consistent with previous classical computer simulations of water using the (rigid) ST2[42] and TIP4P/2005[15] water models. It follows that the present study validates the LLPT hypothesis for water to the case where NQE are included. We note, however, that the LLCP in q-TIP4P/F water, as well as in ST2, TIP4P/2005, and TIP4P/Ice water, is located at pressures and temperatures that are off compared to the experimental predictions[6,46]. This provides a *thermodynamic* explanation of why these water models are unable to reproduce the sharp increase in $C_P(T)$ and $\kappa_T(T)$ observed in experiments at $P = 0.1$ MPa[5,10]. Specifically, these water models predict that $P_c > 150$ MPa, while $P_c \approx 50 - 100$ MPa estimated from experiments[1,50]. Accordingly, computer simulations show a mild increase in κ_T and C_P, relative to experiments, upon isobaric cooling at P = 0.1 MPa. We note that the $C_P(T)$ and $\kappa_T(T)$ quantify the fluctuations in entropy and volume, respectively. Hence, from a *microscopic* point of view, the weak increase of κ_T and C_P upon isobaric cooling at $P = 0.1$ MPa is due to the inability of current water models (ST2, TIP4P/2005, TIP4P/Ice, etc) to reproduce the anomalously large fluctuations (in entropy and volume) of real water in the supercooled regime. At least for the q-TIP4P/F model studied, the inclusion of NQE (quantum fluctuations due to atoms delocalization) is not sufficient to reproduce the anomalously large fluctuations (in entropy and volume) of real water at low temperatures. Accordingly, additional sources of fluctuations may be missed in rigid (e.g., TIP4P/2005, ST2) as well as flexible water models, such as q-TIP4P/F model.

We also performed extensive PIMD simulations of heavy water using the q-TIP4P/F model. The results are summarized in the phase diagram of Fig. 8 (see also the SI). The PIMD simulations confirm that isotope substitution has minor effects on the properties of water. While the phase diagram of D_2O is qualitatively identical to the phase diagram of H_2O, the location of the corresponding LLCP differ. Specifically, calculations based on the TSEOS, applied to PIMD data at $T \geq 190$ K, predict that in the case of D_2O, ($\rho_c = 1.13$ g/cm^3, $P_c = 176$ MPa, $T_c = 177$ K) which represents a non-negligible shift relative to H_2O ($\Delta\rho_c = 0.11$ g/cm^3, $\Delta P_c \approx 9$ MPa, $\Delta T_c \approx 18$ K). This is important since computer simulations of water-like models show that the introduction of NQE can indeed shift considerably the location of the LLCP[47,48]. In particular, the differences in the relative values of (ρ_c, P_c, T_c) between q-TIP4P/F H_2O and D_2O are somewhat consistent with the predictions from experiments in glassy water ($\Delta P_c = 50$ MPa, $\Delta T_c = 10$ K)[49,50] and with the relative location of the κ_T-maximum at 1 bar[10]. The present study shows that many questions previously addressed in computational studies of supercooled water at low temperatures, using classical water models, are accessible via PIMD simulations. For example, it would be interesting to explore the relationship between dynamics and structure of water at low temperatures and how the Stokes–Einstein and Stokes–Einstein–Debye relationships are affected by isotope substitution[82–85].

Data availility

All study data are included in the article and/or SI.

References

1. Gallo, P. *et al.* Water: A tale of two liquids. *Chem. Rev.* **116**, 7463 (2016).
2. Speedy, R. & Angell, C. Isothermal compressibility of supercooled water and evidence for a thermodynamic singularity at - 45 C. *J. Chem. Phys.* **65**, 851 (1976).

3. Angell, C., Shuppert, J. & Tucker, J. Anomalous properties of supercooled water. Heat capacity, expansivity, and proton magnetic resonance chemical shift from 0 to-38%.. *J. Phys. Chem.* **77**, 3092 (1973).
4. Angell, C., Sichina, W. & Oguni, M. Heat capacity of water at extremes of supercooling and superheating. *J. Phys. Chem.* **86**, 998 (1982).
5. Kim, K. H. *et al.* Maxima in the thermodynamic response and correlation functions of deeply supercooled water. *Science* **358**, 1589 (2017).
6. Pathak, H. *et al.* Temperature dependent anomalous fluctuations in water: Shift of 1 kbar between experiment and classical force field simulations. *Mol. Phys.* **117**, 3232 (2019).
7. Poole, P. H., Sciortino, F., Essmann, U. & Stanley, H. E. Phase behaviour of metastable water. *Nature (London)* **360**, 324 (1992).
8. Mishima, O. & Stanley, H. E. The relationship between liquid, supercooled and glassy water. *Nature (London)* **396**, 329 (1998).
9. Kim, K. H. *et al.* Experimental observation of the liquid–liquid transition in bulk supercooled water under pressure. *Science* **370**, 978 (2020).
10. Pathak, H., Späh, A., Esmaeildoost, N., Sellberg, J. A., Kim, K. H., Perakis, F., Amann-Winkel, K., Ladd-Parada, M., Koliyadu, J., Lane, T. J. *et al.* Enhancement and maximum in the isobaric specific-heat capacity measurements of deeply supercooled water using ultrafast calorimetry. *Proc. Natl. Acad. Sci.* **118**, 6 (2021).
11. Suzuki, Y. & Mishima, O. Experimentally proven liquid–liquid critical point of dilute glycerol-water solution at 150 K. *J. Chem. Phys.* **141**, 094505 (2014).
12. Mishima, O. Volume of supercooled water under pressure and the liquid–liquid critical point. *J. Chem. Phys.* **133**, 144503 (2010).
13. Späh, A. *et al.* Apparent power-law behavior of water's isothermal compressibility and correlation length upon supercooling. *Phys. Chem. Chem. Phys.* **21**, 26 (2019).
14. Singh, R. S., Biddle, J. W., Debenedetti, P. G. & Anisimov, M. A. Two-state thermodynamics and the possibility of a liquid–liquid phase transition in supercooled TIP4P/2005 water. *J. Chem. Phys.* **144**, 144504 (2016).
15. González, M. A., Valeriani, C., Caupin, F. & Abascal, J. L. A comprehensive scenario of the thermodynamic anomalies of water using the TIP4P/2005 model. *J. Chem. Phys.* **145**, 054505 (2016).
16. Pallares, G., Gonzalez, M. A., Abascal, J. L. F., Valeriani, C. & Caupin, F. Equation of state for water and its line of density maxima down to - 120 MPa. *Phys. Chem. Chem. Phys.* **18**, 5896 (2016).
17. Pallares, G. *et al.* Anomalies in bulk supercooled water at negative pressure. *Proc. Natl. Acad. Sci.* **111**, 7936 (2014).
18. Debenedetti, P. G., Sciortino, F. & Zerze, G. H. Second critical point in two realistic models of water. *Science* **369**, 289 (2020).
19. Holten, V., Bertrand, C., Anisimov, M. & Sengers, J. Thermodynamics of supercooled water. *J. Chem. Phys.* **136**, 094507 (2012).
20. Holten, V. & Anisimov, M. Entropy-driven liquid–liquid separation in supercooled water. *Sci. Rep.* **2**, 1 (2012).
21. Gartner, T. E. *et al.* Signatures of a liquid–liquid transition in an ab initio deep neural network model for water. *Proc. Natl. Acad. Sci.* **117**, 26040 (2020).
22. Biddle, J. W. *et al.* Two-structure thermodynamics for the TIP4P/2005 model of water covering supercooled and deeply stretched regions. *J. Chem. Phys.* **146**, 034502 (2017).
23. Holten, V., Palmer, J. C., Poole, P. H., Debenedetti, P. G. & Anisimov, M. A. Two-state thermodynamics of the ST2 model for supercooled water. *J. Chem. Phys.* **140**, 104502 (2014).
24. Loerting, T. & Giovambattista, N. Amorphous ices: Experiments and numerical simulations. *J. Phys. Condens. Matter* **18**, R919 (2006).
25. Mishima, O., Calvert, L. & Whalley, E. 'Melting ice' I at 77 K and 10 kbar: A new method of making amorphous solids. *Nature (London)* **310**, 393 (1984).
26. Mishima, O., Calvert, L. & Whalley, E. An apparently first-order transition between two amorphous phases of ice induced by pressure. *Nature (London)* **314**, 76 (1985).
27. Amann-Winkel, K. *et al.* Colloquium: Water's controversial glass transitions. *Rev. Mod. Phys.* **88**, 011002 (2016).
28. Angell, C. A. Amorphous water. *Annu. Rev. Phys. Chem.* **55**, 559 (2004).
29. Wong, J., Jahn, D. A. & Giovambattista, N. Pressure-induced transformations in glassy water: A computer simulation study using the TIP4P/2005 model. *J. Chem. Phys.* **143**, 074501 (2015).
30. Engstler, J. & Giovambattista, N. Heating-and pressure-induced transformations in amorphous and hexagonal ice: A computer simulation study using the TIP4P/2005 model. *J. Chem. Phys.* **147**, 074505 (2017).
31. Giovambattista, N., Loerting, T., Lukanov, B. R. & Starr, F. W. Interplay of the glass transition and the liquid–liquid phase transition in water. *Sci. Rep.* **2**, 1 (2012).
32. Giovambattista, N., Starr, F. W. & Poole, P. H. State variables for glasses: The case of amorphous ice. *J. Chem. Phys.* **150**, 224502 (2019).
33. Martelli, F., Giovambattista, N., Torquato, S. & Car, R. Searching for crystal-ice domains in amorphous ices. *Phys. Rev. Mater.* **2**, 075601 (2018).
34. Handle, P. H., Sciortino, F. & Giovambattista, N. Glass polymorphism in TIP4P/2005 water: A description based on the potential energy landscape formalism. *J. Chem. Phys.* **150**, 244506 (2019).
35. Sastry, S., Debenedetti, P. G., Sciortino, F. & Stanley, H. E. Singularity-free interpretation of the thermodynamics of supercooled water. *Phys. Rev. E* **53**, 6144 (1996).
36. Mishima, O. Reversible first-order transition between two H_2O amorphs at 0.2 GPa and 135 K. *J. Chem. Phys.* **100**, 5910 (1994).
37. Amann-Winkel, K. *et al.* Water's second glass transition. *Proc. Natl. Acad. Sci.* **110**, 17720 (2013).
38. Palmer, J. C. *et al.* Metastable liquid–liquid transition in a molecular model of water. *Nature (London)* **510**, 385 (2014).
39. Palmer, J. C., Car, R. & Debenedetti, P. G. The liquid–liquid transition in supercooled ST2 water: A comparison between umbrella sampling and well-tempered metadynamics. *Faraday Discuss.* **167**, 77 (2013).
40. Palmer, J. C., Poole, P. H., Sciortino, F. & Debenedetti, P. G. Advances in computational studies of the liquid–liquid transition in water and water-like models. *Chem. Rev.* **118**, 9129 (2018).
41. Liu, Y., Palmer, J. C., Panagiotopoulos, A. Z. & Debenedetti, P. G. Liquid–liquid transition in ST2 water. *J. Chem. Phys.* **137**, 2140505 (2012).
42. Poole, P. H., Saika-Voivod, I. & Sciortino, F. Density minimum and liquid–liquid phase transition. *J. Phys. Condens. Matter* **17**, L431 (2005).
43. Handle, P. H. & Sciortino, F. Potential energy landscape of TIP4P/2005 water. *J. Chem. Phys.* **148**, 134505 (2018).
44. Poole, P. H., Bowles, R. K., Saika-Voivod, I. & Sciortino, F. Free energy surface of ST2 water near the liquid–liquid phase transition. *J. Chem. Phys.* **138**, 034505 (2013).
45. Ceriotti, M. *et al.* Nuclear quantum effects in water and aqueous systems: Experiment, theory, and current challenges. *Chem. Rev.* **116**, 7529 (2016).
46. Eltareb, A., Lopez, G. E. & Giovambattista, N. Nuclear quantum effects on the thermodynamic, structural, and dynamical properties of water. *Phys. Chem. Chem. Phys.* **23**, 6914 (2021).
47. Liu, Y. *et al.* Nuclear quantum effects on the thermodynamic response functions of a polymorphic waterlike monatomic liquid. *Phys. Rev. Res.* **2**, 013153 (2020).
48. Nguyen, B., Lopez, G. E. & Giovambattista, N. Nuclear quantum effects on the liquid–liquid phase transition of a water-like monatomic liquid. *Phys. Chem. Chem. Phys.* **20**, 8210 (2018).

49. Mishima, O. & Stanley, H. E. Decompression-induced melting of ice IV and the liquid–liquid transition in water. *Nature (London)* **392**, 164 (1998).
50. Mishima, O. Liquid–liquid critical point in heavy water. *Phys. Rev. Lett.* **85**, 334 (2000).
51. Caupin, F. & Anisimov, M. A. Thermodynamics of supercooled and stretched water: Unifying two-structure description and liquid-vapor spinodal. *J. Chem. Phys.* **151**, 034503 (2019).
52. Duboué-Dijon, E. & Laage, D. Characterization of the local structure in liquid water by various order parameters. *J. Phys. Chem. B* **119**, 8406 (2015).
53. Ansari, N., Dandekar, R., Caravati, S., Sosso, G. & Hassanali, A. High and low density patches in simulated liquid water. *J. Chem. Phys.* **149**, 204507 (2018).
54. Habershon, S., Markland, T. E. & Manolopoulos, D. E. Competing quantum effects in the dynamics of a flexible water model. *J. Chem. Phys.* **131**, 024501 (2009).
55. Abascal, J. L. & Vega, C. A general purpose model for the condensed phases of water: TIP4P/2005. *J. Chem. Phys.* **123**, 234505 (2005).
56. Ceriotti, M., Parrinello, M., Markland, T. E. & Manolopoulos, D. E. Efficient stochastic thermostatting of path integral molecular dynamics. *J. Chem. Phys.* **133**, 124104 (2010).
57. Eastman, P. *et al.* OpenMM 4: A reusable, extensible, hardware independent library for high performance molecular simulation. *J. Chem. Theory Comput.* **9**, 461 (2013).
58. Holten, V., Limmer, D. T., Molinero, V. & Anisimov, M. A. Nature of the anomalies in the supercooled liquid state of the mW model of water. *J. Chem. Phys.* **138**, 174501 (2013).
59. Wagner, W. & Pruß, A. The IAPWS formulation 1995 for the thermodynamic properties of ordinary water substance for general and scientific use. *J. Phys. Chem. Ref. Data* **31**, 387 (2002).
60. Kell, G. Precise representation of volume properties of water at one atmosphere. *J. Chem. Eng. Data* **12**, 66 (1967).
61. Hare, D. & Sorensen, C. Densities of supercooled H_2O and D_2O in 25 μ glass capillaries. *J. Chem. Phys.* **84**, 5085 (1986).
62. Callen, H. B. *Thermodynamics and an Introduction to Thermostatistics.* (Wiley, 2006).
63. Pathria, R. & Beale, P. D. *Statistical Mechanics* (Elsevier, 2011).
64. Abascal, J. L. & Vega, C. Widom line and the liquid–liquid critical point for the TIP4P/2005 water model. *J. Chem. Phys.* **133**, 234502 (2010).
65. Kanno, H. & Angell, C. Water: Anomalous compressibilities to 1.9 kbar and correlation with supercooling limits. *J. Chem. Phys.* **70**, 4008 (1979).
66. Kell, G. S. Density, thermal expansivity, and compressibility of liquid water from 0. deg. to 150. deg. Correlations and tables for atmospheric pressure and saturation reviewed and expressed on 1968 temperature scale.. *J. Chem. Eng. Data* **20**, 97 (1975).
67. Ter Minassian, L., Pruzan, P. & Soulard, A. Thermodynamic properties of water under pressure up to 5 kbar and between 28 and 120 C. Estimations in the supercooled region down to - 40 C.. *J. Chem. Phys.* **75**, 3064 (1981).
68. Vega, C. *et al.* Heat capacity of water: A signature of nuclear quantum effects. *J. Chem. Phys.* **132**, 046101 (2010).
69. Troncoso, J. The isobaric heat capacity of liquid water at low temperatures and high pressures. *J. Chem. Phys.* **147**, 084501 (2017).
70. Harris, K. R. & Woolf, L. A. Pressure and temperature dependence of the self diffusion coefficient of water and oxygen-18 water. *J. Chem. Soc. Faraday Trans.* **76**, 377 (1980).
71. Prielmeier, F., Lang, E., Speedy, R. & Lüdemann, H.-D. Diffusion in supercooled water to 300 MPa. *Phys. Rev. Lett.* **59**, 1128 (1987).
72. Poole, P. H., Sciortino, F., Essmann, U. & Stanley, H. E. Spinodal of liquid water. *Phys. Rev. E* **48**, 3799 (1993).
73. Torre, R., Bartolini, P. & Righini, R. Structural relaxation in supercooled water by time-resolved spectroscopy. *Nature (London)* **428**, 296 (2004).
74. Gordon, A. & Giovambattista, N. Glass transitions in a monatomic liquid with two glassy states. *Phys. Rev. Lett.* **112**, 145701 (2014).
75. Gartner, T. E., Torquato, S., Car, R. & Debenedetti, P. G. Manifestations of metastable criticality in the long-range structure of model water glasses. *Nat. Commun.* **12**, 1 (2021).
76. Smallenburg, F., Poole, P. H. & Sciortino, F. Phase diagram of the ST2 model of water. *Mol. Phys.* **113**, 2791 (2015).
77. Horstmann, R. & Vogel, M. Relations between thermodynamics, structures, and dynamics for modified water models in their supercooled regimes. *J. Chem. Phys.* **154**, 054502 (2021).
78. Henderson, S. J. & Speedy, R. J. Temperature of maximum density in water at negative pressure. *J. Phys. Chem.* **91**, 3062 (1987).
79. Vedamuthu, M., Singh, S. & Robinson, G. W. Properties of liquid water. 4. The isothermal compressibility minimum near 50. degree. C.. *J. Phys. Chem.* **99**, 9263 (1995).
80. Holten, V. *et al.* Compressibility anomalies in stretched water and their interplay with density anomalies. *J. Phys. Chem. Lett.* **8**, 5519 (2017).
81. Kanno, H. & Angell, C. Volumetric and derived thermal characteristics of liquid D_2O at low temperatures and high pressures. *J. Chem. Phys.* **73**, 1940 (1980).
82. Zhang, C. & Galli, G. Dipolar correlations in liquid water. *J. Chem. Phys.* **141**, 084504 (2014).
83. Ansari, N., Onat, B., Sosso, G. C. & Hassanali, A. Insights into the emerging networks of voids in simulated supercooled water. *J. Phys. Chem. B* **124**, 2180 (2020).
84. Mazza, M. G., Giovambattista, N., Stanley, H. E. & Starr, F. W. Connection of translational and rotational dynamical heterogeneities with the breakdown of the Stokes–Einstein and Stokes–Einstein–Debye relations in water. *Phys. Rev. E* **76**, 031203 (2007).
85. Ragueneau, P., Caupin, F., & Issenmann, B. Shear viscosity and Stokes–Einstein violation in supercooled light and heavy water. arXiv:2112.09024 (2021).

Acknowledgements

Author contributions

N.G. and G.E.L. designed research; A.E. performed research; A.E., G.E.L., and N.G. analyzed data; and A.E., G.E.L., and N.G. wrote the paper.

Competing interests

The authors declare no competing interests.

Additional information

Supplementary Information The online version contains supplementary material available at https://doi.org/10.1038/s41598-022-09525-x.

Correspondence and requests for materials should be addressed to A.E.

Reprints and permissions information is available at www.nature.com/reprints.

Publisher's note Springer Nature remains neutral with regard to jurisdictional claims in published maps and institutional affiliations.